

Flat bands and unconventional superconductivity in a simple model of metal-organic frameworks

M. F. Ohlrich,^{1,*} E. M. Makarez,¹ H. L. Nourse,² and B. J. Powell¹

¹*School of Mathematics and Physics, The University of Queensland, 4072, Australia*

²*Quantum Information Science and Technology Unit,*

Okinawa Institute of Science and Technology Graduate University, Onna-son, Okinawa 904-0495, Japan

The superconducting metal-organic framework Cu-BHT forms a kagome lattice with metals at the vertices and ligands along the bonds. This bipartite motif is common in reticular materials. We show that a tight-binding model on this lattice yields partially occupied interference-induced flat bands at half-filling with large gaps between them and all other bands. Long-range hopping induces curvature in the bands but leaves them flatter and more isolated than those in twisted bilayer graphene. The slave boson theory of the t - J model on this lattice shows highly unconventional superconductivity including an f -wave singlet phase. Thus, framework materials provide an ideal lattice-driven approach to strongly correlated phenomena in flat bands at high electronic densities.

Reticular materials are crystalline frameworks built by linking molecular building blocks with strong (e.g., covalent, dative) bonds; metal-organic frameworks (MOFs), coordination polymers (CPs) and covalent organic frameworks (COFs) provide prominent examples [1]. Many correlated insulating states occur in reticular materials [2–9]. Therefore, it has been argued that these systems may display unconventional superconductivity when driven out of their insulating phases, e.g., by doping [10], pressure, or control of chemistry [11]. This hypothesis received strong support from the recent discovery of superconductivity in copper(II) benzenehexathiolate (Cu-BHT) [12], and from the evidence of unconventional superconductivity and strong electronic correlations in this material [13].

Contemporaneously, the discovery of superconductivity and strongly correlated insulating states in twisted bilayer graphene (TBG) revived interest in flat band superconductivity [14, 15]. In TBG, a group of isolated ‘nearly flat bands’, with a total bandwidth on the order of 10 meV, and band gaps of the same order on either side [14, 16], cross the Fermi energy. In a flat band, the kinetic energy of all electrons is equal. Thus, interactions determine the behavior of the system, amplifying strongly correlated phenomena, such as the fractional quantum Hall effect, high temperature superconductivity, and metal-insulator transitions [17, 18]. However, TBG has extremely low electron densities, and many of the most interesting predictions for flat bands require high electron densities [17, 19]. Thus, discovering bulk materials with flat bands is an important goal.

In this Letter, we argue that reticular materials generically form bipartite lattices with flat bands, which can be understood as a consequence of Sutherland’s theorem [20, 21]. We explore a simple example; the kagome-Lieb lattice, Fig. 1a, which is to the kagome lattice as the Lieb lattice is to the square lattice. We show that an s -orbital model on this lattice has five interference-induced flat

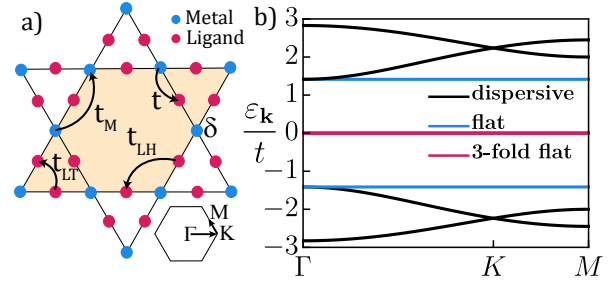


FIG. 1. Tight-binding model on the kagome-Lieb lattice. (a) Hopping integrals are marked, δ is the site energy of the metals, and the shaded area is the unit cell. The Bravais lattice is inset; Γ , M and K label the high symmetry points. (b) Band structure of the nearest-neighbor model.

bands (IFBs), three of which are partially occupied at half-filling, with large gaps between them and all other bands Fig. 1b. We show that, and explain why, they are robust to the largest expected perturbations. The multi-orbital analogue has a closely related band structure with IFBs, which can be understood in terms of the single band model, and reproduces the key features of the band structure of the superconducting MOF, Cu-BHT, in which the metals form a kagome lattice with ligand sites along the bonds. When strong electronic correlations are included, we find that the s -orbital model leads to competing unconventional superconducting phases, including an f -wave singlet state, enabled by the rich structure of the lattice.

General arguments suggest reticular materials are ideally suited for the study of flat band physics. CPs consist of metallic centers bonded to organic groups (ligands) [1]. These ligands link to other metals to form a crystal. It is straightforward to prove that, for simple connected lattices in more than one dimension, the number of ligands must be greater than the number of metals. The large unit cells of CPs mean that beyond nearest-neighbor hopping is often negligible, resulting in bipartite lattices. Whence Sutherland’s theorem [20] immediately requires $N_L - N_M$ zero energy flat bands, where N_L (N_M) is the

* miriam.ohlrich@uq.net.au

number of ligand (metal) orbitals per unit cell. MOFs are the subclass of CPs with high porosity [22], and hence have widespread potential applications, such as carbon capture and storage, hydrogen fuel storage, microelectronics, and drug delivery [2, 3, 22]. COFs are similar to CPs and MOFs, but with the metals replaced by an organic group [4, 23]. Therefore, one also expects zero energy flat bands in MOFs and COFs. ‘Crystal engineering’ [24, 25]: the rational design of the crystal structures of reticular materials is enabled by the local nature of chemical bonding [1, 24–27]. Thus, realizing specific lattice structures in reticular materials is a highly achievable objective. Furthermore, reticular lattice structures could also be realized in optical lattices.

To substantiate these ideas, we explore an example. In many CPs and MOFs, including Cu-BHT [12, 13], the metals form a kagome lattice with the ligands lying along the nearest-neighbor bonds [28–30]. For example, in Cu-BHT, density functional theory (DFT) shows that the low-energy electronic structure is dominated by bands that originate from the Cu and S atoms with little weight on the C atoms [11]; structurally, the S atoms sit along the nearest-neighbor Cu-Cu bonds. As both the metals and ligands have orbitals near the Fermi energy, the simplest possible model is the tight-binding model on the kagome-Lieb lattice, Fig. 1a. Importantly, increasing covalency between metals and ligands is a design strategy for achieving metallic and superconducting MOFs [2], which motivated the first studies of Cu-BHT [13], and necessitates electronic models including both the metals and the ligands. This lattice also occurs quite naturally in COFs [23]. In contrast, the kagome-Lieb lattice structure is absent from a recent catalog of flat-band inorganic materials [19]. Thus, we study the Hamiltonian

$$H_{tb} = - \sum_{i,j,\mu,\nu,\sigma} t_{ij}^{\mu\nu} \hat{c}_{i\mu\sigma}^\dagger \hat{c}_{j\nu\sigma} + \sum_{i \in M, \mu, \sigma} \delta_{\mu} \hat{c}_{i\mu\sigma}^\dagger \hat{c}_{i\mu\sigma}, \quad (1)$$

where $\hat{c}_{i\mu\sigma}^{(\dagger)}$ creates (annihilates) an electron of spin σ in orbital μ at site i , $t_{ij}^{\mu\nu}$ is the hopping amplitude between orbitals at different sites, and ligand-ligand sites, and the sum over $i \in M$ includes metal sites only.

Generically, reticular materials will be multi-orbital, but we can learn a lot about the kagome-Lieb lattice structure by considering its simplest version with one s -orbital per site: we suppress the orbital indices and sketch the hopping amplitudes $t_{ij}^{\mu\nu} \in \{t, t_M, t_{LH}, t_{LT}\}$ in Fig. 1a. Although there are nine sites per unit cell, we were able to solve this model analytically.

In the nearest-neighbor model ($\delta = t_M = t_{LH} = t_{LT} = 0$) there are five IFBs: three degenerate IFBs at $\varepsilon_{\mathbf{k}} = 0$ and two ‘kagome-like’ IFBs, which touch kagome-like dispersive bands (Fig. 1b). The three degenerate flat bands are required by Sutherland’s theorem [20] for $N_L = 6$, $N_M = 3$; however, the kagome-like flat bands are not.

The five flat bands result from quantum interference due to the topology of the lattice and are thus IFBs [18, 31–34]. The localized states that comprise the flat-band of the kagome lattice consist of alternating sign

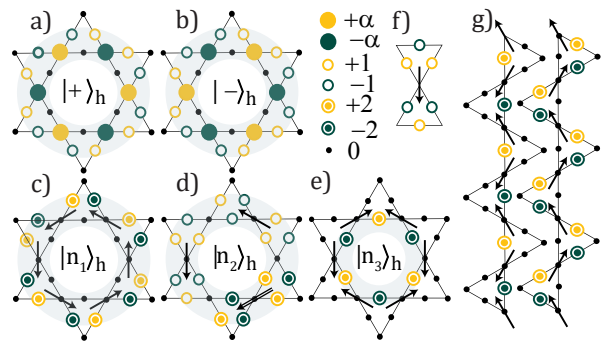


FIG. 2. (Unnormalized) localized eigenstates for each of the interference-induced flat bands. Electrons cannot hop outside the loops due to destructive interference. The (a) antibonding $(|+\rangle_h)$ and (b) bonding $(|-\rangle_h)$ kagome-like eigenstates have energies $E_{\pm} = [t_{LT} + 2t_M + \delta \pm \sqrt{8t^2 + (2t_M - t_{LT} + \delta)^2}]/2$ and a relative amplitude on the metal sites of $\alpha_{\pm} = (E_{\pm} - t_{LT})/t$ (for $t_{LH} = 0$). The three non-bonding (between metals and ligands) eigenstates (c-e) can be constructed as superpositions of bow-tie states (f), as can noncontractable loops for PBC (g). The superpositions are indicated by the arrows which define the sign of the bow-tie wavefunctions centered on each metal site.

amplitudes around each hexagon [31]. The kagome-like IFBs on the kagome-Lieb lattice are composed of the (anti)bonding combination of the metals and two nearest-neighbor ligands on hexagon h . These hybrid orbitals form flat bands, $(|+\rangle_h)$ $(|-\rangle_h)$, analogous to those found in the kagome lattice (Fig. 2a,b). The dispersive bands with (high) low energies are also kagome bands in the basis of the (anti)bonding states of metals/nearest-neighbor ligands. This explains the Dirac point at K (Fig. 1b). In contrast, the three degenerate IFBs are non-bonding (between metals and ligands), as they have no weight on the metal sites (Fig. 2c-e). The non-bonding states can also be understood as superpositions of ‘bow-tie’ states Fig. 2f.

The two kagome-like flat bands are singular as they touch a dispersive band at the Γ point ($k = 0$). This has a simple explanation, analogous to that for the kagome [31] and other decorated kagome lattices [33]. Each unit cell contains one hexagon (Fig. 1). Therefore, for N unit cells and open boundary conditions (OBC) there are N (anti)bonding kagome-like IFB states. Superpositions of $(|\pm\rangle_h)$ states on adjacent hexagons have zero weight on the sites that contribute to both localized wavefunctions due to destructive interference. Therefore, $\sum_h |+\rangle_h = \sum_h |-\rangle_h = 0$ for periodic boundary conditions (PBC), leaving $N - 1$ non-trivial superpositions of $(|\pm\rangle_h)$. However, for PBC one can construct two additional states, which cannot be written as superpositions of $(|\pm\rangle_h)$ ($(|-\rangle_h)$), and wrap around the lattice (i.e., one noncontractable loop composed of (anti)bonding states in each of the x and y directions) [31, 33]; resulting in $N + 1$ states with energy E_{\pm} . As each IFB can only accommodate N states, topology dictates that there cannot be

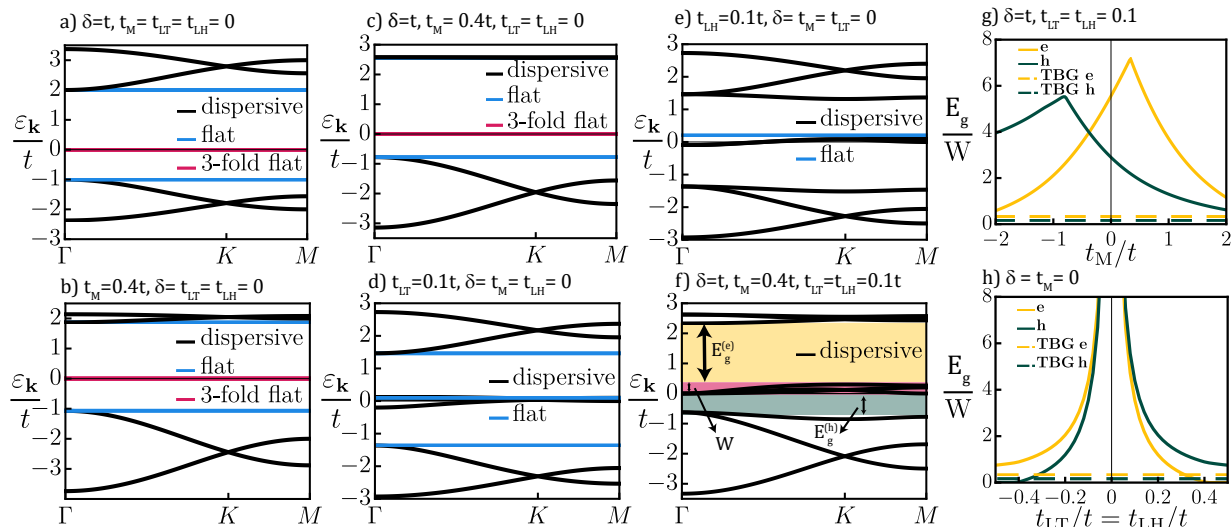


FIG. 3. Evolution of the band structure of the kagome-Lieb lattice tight-binding model with hopping beyond nearest-neighbors. Five bands remain exactly flat even when (a) metal-ligand orbital energy differences, δ , (b) direct metal-metal hopping, t_M , or (c) both are included. (d) Ligand-ligand hopping across triangles, t_{LT} , leaves three exactly flat bands. (e) Ligand-ligand hopping across hexagons, t_{LH} , leaves one flat band. (f) Including all of these terms leaves no bands exactly flat, but the non-bonding bands remain gapped and narrow. The bandwidth of the non-bonding bands (W), the electron bandgap ($E_g^{(e)}$) and the hole bandgap ($E_g^{(h)}$) are labeled. (g,h) For a wide range of parameters, even for large t_M , t_{LT} and t_{LH} , the non-bonding bands remain much flatter and more isolated (i.e., have larger E_g/W) than the nearly-flat bands in TBG (from Ref. 16).

a gap between the kagome-like IFBs and the dispersive bands.

The non-bonding states are most easily counted in the basis of bow-tie states (Fig. 2f). There are three metal sites, and thus three bow-tie states, per unit cell. No non-trivial superposition of the bow-ties vanishes. All noncontractable loops are superpositions of bow-ties (Fig. 2g). Thus, the $3N$ bow-tie states are non-singular and need not touch a dispersive band.

The non-singularity of the non-bonding IFBs allows significant gaps between the non-bonding IFBs and the dispersive bands. In contrast, the IFBs on the kagome [31], Lieb [32], pyrochlore [31], and star [33] lattices are all singular and have topologically required band touchings, and therefore, excitations into dispersive bands occur at arbitrarily low energies. Thus, materials realizing these lattices are significantly less promising candidates to explore flat band physics at high electronic densities than materials that form kagome-Lieb lattices. New reticular materials tailored to exploit this structure could be readily synthesized to compliment existing examples, such as Cu-BHT.

Although the nearest-neighbor model is realizable via ultracold gases in optical lattices, additional terms are likely relevant to reticular materials. A mismatch in the orbital energies of the metals and ligands, $\delta \neq 0$, does not induce a curvature in the degenerate IFBs as the lattice remains bipartite, (and, more intuitively, none of the localized wavefunctions contain any amplitude on the metals, Fig. 2c-e) [20]. The two kagome-like IFBs remain, as δ simply changes the amplitudes on the metal and ligand

orbitals in the (anti)bonding orbitals. However, $\delta \neq 0$ breaks particle-hole symmetry; positive δ increases (decreases) the energy gap between the non-bonding IFBs and the (anti)bonding kagome-like bands, $E_g^{(h)}$ ($E_g^{(e)}$).

Direct metal-metal hopping, t_M , does not cause any of the five IFBs of the kagome-Lieb lattice to become dispersive, Fig. 3b. This is surprising as the lattice is no longer bipartite for $t_M \neq 0$. Therefore, Sutherland's theorem no longer guarantees that the model retains the three non-bonding IFBs. However, as the non-bonding IFBs have zero amplitude on all metal sites, metal-metal hopping cannot perturb them. The two kagome-like IFBs have non-zero amplitudes on the metal sites. However, in $|+\rangle_h$ and $|-\rangle_h$, the phases of the metal sites alternate around each hexagon and are therefore localized by destructive interference under direct metal-metal hopping, Fig. 2. Therefore, the contribution to the energy of kagome-like IFBs from metal-metal hopping is independent of momentum and these bands remain completely flat.

Thus, the five IFBs remain completely dispersionless, regardless of the values of δ and t_M , Fig. 3a-c. This is important because the values for δ and t_M in CPs and MOFs can vary dramatically, even between closely related materials [35].

Direct ligand-ligand hopping is typically small; however, it is not always negligible [6, 36]. We consider ligand-ligand hoppings across triangles, t_{LT} , and across hexagons, t_{LH} ; Fig. 1a. For example, the latter could be mediated by virtual hopping via the $S-p_z$ orbitals in Cu-BHT. Both have important qualitative effects on the

band structure of the kagome-Lieb lattice, Fig. 3d-f. If exactly one of t_{LT} and t_{LH} is non-zero only one of the non-bonding IFBs remains exactly flat. This can be understood from interference and lattice topology as a simple extension of the above arguments [37].

For both $t_{LT} \neq 0$ and $t_{LH} \neq 0$, no completely flat bands remain, Fig. 3f. However, the non-bonding bands remain nearly flat and widely gapped, indeed, significantly flatter and more isolated than the nearly flat bands in TBG, Fig. 3g,h.

The large unit cells of reticular materials mean that longer range hopping is likely to be negligible. Thus we expect that these conclusions will hold in many framework materials described by kagome-Lieb lattice tight-binding models.

It is also interesting to anticipate future experiments where a 2D kagome-Lieb material is grown on a substrate. Strain caused by the substrate will perturb the ideal lattice and hence the hopping parameters. The non-bonding IFBs will even be robust to such distortions because they do not change the bipartite nature of the lattice so Sutherland's theorem still holds.

The multi-orbital tight-binding model (Eq. 1) with a Slater-Koster parameterization [37] reproduces many features of the DFT band structure of Cu-BHT [11], Fig. 4. The multi-orbital tight-binding model hosts several flat and nearly flat bands, which can readily be understood from simple generalizations of the arguments above. The model is symmetric under reflection through the plane and hence is separable into even (odd) sectors, with support from ligand π_x and π_y orbitals, and metal d_{xy} , $d_{x^2-y^2}$ and d_{z^2} (ligand π_z and metal d_{xz} and d_{yz}) orbitals. The d_{z^2} orbitals are energetically separated and do not hybridize significantly with the other orbitals in Cu-BHT; therefore we neglect them below. This leaves 12 (6) ligand and 6 (6) metal orbitals per unit cell in the even (odd) sector. Therefore, we expect 6 even non-bonding IFBs with support on the π_x and π_y orbitals (Fig. 4).

There are twice as many IFBs in the even sector of the multiband model as there are in the s -orbital model because there are two orbitals per site in the even sector. The compact localised states that give rise to the IFBs in the multiorbital model are simply related to those that give rise to the non-bonding IFBs in the s -orbital model: the single orbitals are replaced by a superposition of the two orbitals on a given site. This leads to a deep connection between the resulting IFBs in the two models: both are required by Sutherland's theorem, are robust to strain, remain exactly flat when metal-metal hopping is added even though the lattice is no longer bipartite, and remain very narrow when ligand-ligand hopping is added [37].

To understand the role of electronic correlations we study the nearest-neighbor s -orbital kagome-Lieb t - J model:

$$H_{tJ} = \hat{P} \left[H_{tb} + J \sum_{\langle i,j \rangle_1} \hat{S}_i \cdot \hat{S}_j \right] \hat{P}, \quad (2)$$

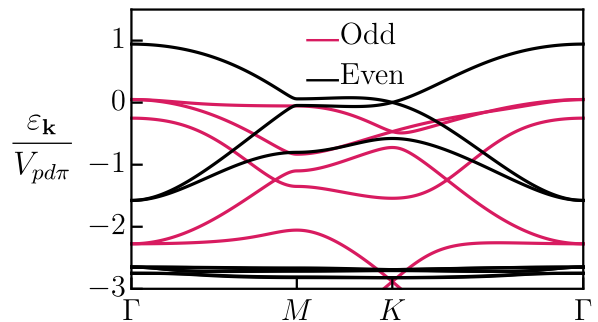


FIG. 4. Nearly flat interference-induced bands remain in a multi-orbital kagome-Lieb lattice model, with d -orbitals on the metals and π -orbitals on the ligands [37]. Here we show the model for parameters chosen to reproduce the key features of the band structure of Cu-BHT (cf. Ref. [11]). $V_{pd\pi}$ is a Slater-Koster energy integral [37–39].

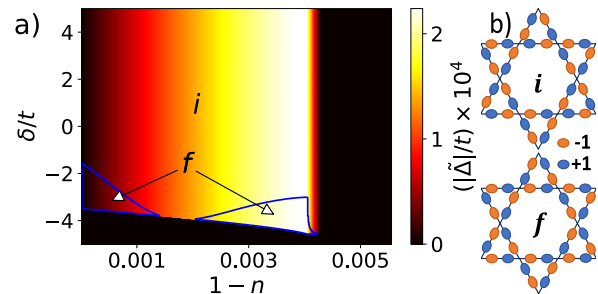


FIG. 5. (a) Two competing unconventional superconducting phases emerge when hole doping from the half-filled three degenerate flat bands. (Note the lattice is particle-hole symmetric.) Blue lines represent first order phase transitions. Here $J = 0.2t$, n is the electron density per site, and $\tilde{\Delta}$ is the superconducting order parameter. (b) Sketches of the superconducting order parameters.

where \hat{P} is the Gutzwiller projector and \hat{S}_i is the spin operator on site i . We write the electronic operators $\hat{c}_{i\sigma} = \hat{b}_i^\dagger \hat{f}_{i\sigma}$ in terms of (slave) bosonic holons, \hat{b}_i , and fermionic quasiparticles, $\hat{f}_{i\sigma}$ [40] and calculate the superconducting order parameter, $\tilde{\Delta}_{ij} = (3J/8) \langle \hat{b}_i^\dagger \hat{b}_j^\dagger \rangle \langle \hat{f}_{i\uparrow} \hat{f}_{j\downarrow} - \hat{f}_{i\downarrow} \hat{f}_{j\uparrow} \rangle$, in the mean-field approximation [37, 41].

We find two competing unconventional superconducting states: $f \sim x(x^2 - 3y^2)$ and $i \sim xy(3x^4 - 10x^2y^2 + 3y^4)$, Fig. 5b. While $\tilde{\Delta} \neq 0$ indicates condensing Cooper pairs, a non-zero superfluid stiffness is required to exhibit the Meissner effect. For an isolated set of partially filled flat bands the superfluid stiffness in the weak coupling limit is given by $D_s \propto \text{tr}(g)|\tilde{\Delta}|$, where g is the minimal Fubini-Study quantum metric [18, 42–46]. The equivalent condition for strong coupling superconductivity remains an open question. We find $\text{tr}(g) = 0.13(9)$ for the parameters in Fig. 3f. Thus, we expect a non-zero superfluid stiffness in the superconducting phases.

On a simple lattice an f -wave singlet phase is incom-

patible with Fermi statistics. But the f -wave singlet we find is odd under spatial inversion, spin inversion, and sublattice inversion, yielding a totally antisymmetric wavefunction. This suggests that such highly unconventional superconductivity might be commonplace in CPs, MOFs, and COFs [10].

This demonstrates that the very narrow, isolated bands in materials with the kagome-Lieb lattice structure exhibit exotic, strongly correlated phenomena, including unconventional superconductivity. Thus, the kagome-

Lieb lattice is an unusually rich playground for unconventional superconductivity. This provides strong support for our central hypothesis that reticular materials are an ideal platform for investigating flat band physics. A key design principle, derived from the results above, is to choose ligands with low direct ligand-ligand overlap as this minimizes the bandwidth of the non-bonding bands.

This work was supported by the Australian Research Council (DP180101483) and MEXT Quantum Leap Flagship Program (MEXT Q-LEAP) Grant Number JP-MXS0118069605.

-
- [1] M. J. Kalmutzki, N. Hanikel, and O. M. Yaghi, Secondary building units as the turning point in the development of the reticular chemistry of MOFs, *Sci. Adv.* **4**, eaat9180 (2018).
- [2] L. Sun, M. G. Campbell, and M. Dincă, Electrically conductive porous metal-organic frameworks, *Angew. Chem. Int. Ed.* **55**, 3566 (2016).
- [3] M. B. Solomon, T. L. Church, and D. M. D'Alessandro, Perspectives on metal-organic frameworks with intrinsic electrocatalytic activity, *Cryst. Eng. Comm.* **19**, 4049 (2017).
- [4] K. Geng, T. He, R. Liu, S. Dalapati, K. T. Tan, Z. Li, S. Tao, Y. Gong, Q. Jiang, and D. Jiang, Covalent organic frameworks: Design, synthesis, and functions, *Chem. Rev.* **120**, 8814 (2020).
- [5] R. Murase *et al.*, Multi-redox responsive behavior in a mixed-valence semiconducting framework based on bis-[1,2,5]-thiadiazolo-tetracyanoquinodimethane, *J. Am. Chem. Soc.* **144**, 13242 (2022).
- [6] D. Kumar, J. Hellerstedt, B. Field, B. Lowe, Y. Yin, N. V. Medhekar, and A. Schiffrin, Manifestation of strongly correlated electrons in a 2D kagome metal-organic framework, *Adv. Funct. Mater.* **31**, 2106474 (2021).
- [7] H. L. Nourse, R. H. McKenzie, and B. J. Powell, Multiple insulating states due to the interplay of strong correlations and lattice geometry in a single-orbital Hubbard model, *Phys. Rev. B* **103**, L081114 (2021).
- [8] H. L. Nourse, R. H. McKenzie, and B. J. Powell, Spin-0 Mott insulator to metal to spin-1 Mott insulator transition in the single-orbital Hubbard model on the decorated honeycomb lattice, *Phys. Rev. B* **104**, 075104 (2021).
- [9] H. L. Nourse, R. H. McKenzie, and B. J. Powell, C_3 symmetry breaking metal-insulator transitions in a flat band in the half-filled Hubbard model on the decorated honeycomb lattice, *Phys. Rev. B* **105**, 205119 (2022).
- [10] J. Merino, M. F. López, and B. J. Powell, Unconventional superconductivity near a flat band in organic and organometallic materials, *Phys. Rev. B* **103**, 094517 (2021).
- [11] X. Zhang, Y. Zhou, B. Cui, M. Zhao, and F. Liu, Theoretical discovery of a superconducting two-dimensional metal-organic framework, *Nano Lett.* **17**, 6166 (2017).
- [12] X. Huang, S. Zhang, L. Liu, L. Yu, G. Chen, W. Xu, and D. Zhu, Superconductivity in a copper(II)-based coordination polymer with perfect kagome structure, *Angew. Chem. Int. Ed.* **57**, 146 (2018).
- [13] T. Takenaka *et al.*, Strongly correlated superconductivity in a copper-based metal-organic framework with a perfect kagome lattice, *Sci. Adv.* **7** (2021).
- [14] Y. Cao, V. Fatemi, S. Fang, K. Watanabe, T. Taniguchi, E. Kaxiras, and P. Jarillo-Herrero, Unconventional superconductivity in magic-angle graphene superlattices, *Nature* **556**, 43 (2018).
- [15] Y. Cao *et al.*, Correlated insulator behaviour at half-filling in magic-angle graphene superlattices, *Nature* **556**, 80 (2018).
- [16] S. Pathak, T. Rakib, R. Hou, A. Nevidomskyy, E. Ertekin, H. T. Johnson, and L. K. Wagner, Accurate tight-binding model for twisted bilayer graphene describes topological flat bands without geometric relaxation, *Phys. Rev. B* **105**, 115141, (2022).
- [17] L. Balents, C. R. Dean, D. K. Efetov, and A. F. Young, Superconductivity and strong correlations in moiré flat bands, *Nat. Phys.* **16**, 725 (2020).
- [18] P. Törmä, S. Peotta, and B. A. Bernevig, Superconductivity, superfluidity and quantum geometry in twisted multilayer systems, *Nat. Rev. Phys.* **4**, 528 (2022).
- [19] N. Regnault *et al.*, Catalogue of flat-band stoichiometric materials, *Nature* **603**, 824 (2022).
- [20] B. Sutherland, Localization of electronic wave functions due to local topology, *Phys. Rev. B* **34**, 5208 (1986).
- [21] D. Călugăru, A. Chew, L. Elcoro, Y. Xu, N. Regnault, Z.-D. Song, and B. A. Bernevig, General construction and topological classification of crystalline flat bands, *Nat. Phys.* **18**, 185–189 (2021).
- [22] H. Furukawa, K. E. Cordova, M. O’Keeffe, and O. M. Yaghi, The chemistry and applications of metal-organic frameworks, *Science* **341**, 1230444 (2013).
- [23] M. S. Lohse and T. Bein, Covalent organic frameworks: Structures, synthesis, and applications, *Adv. Funct. Mater.* **28**, 1705553 (2018).
- [24] R. Robson, A net-based approach to coordination polymers, *J. Chem. Soc., Dalton Trans.* **2000**, 3735 (2000).
- [25] R. Robson, Design and its limitations in the construction of bi- and poly-nuclear coordination complexes and coordination polymers (aka MOFs): a personal view, *Dalton Trans.* **2008**, 5113 (2008).
- [26] O. M. Yaghi, M. O’Keeffe, N. W. Ockwig, H. K. Chae, M. Eddaoudi, and J. Kim, *Nature* **423**, 705–714 (2003).
- [27] B. Cui, X. Zheng, J. Wang, D. Liu, S. Xie, and B. Huang, Realization of Lieb lattice in covalent-organic frameworks with tunable topology and magnetism, *Nat. Commun.* **11**, 66 (2020).

- [28] M. Hua *et al.*, Highly degenerate ground states in a frustrated antiferromagnetic kagome lattice in a two-dimensional metal-organic framework, *J. Phys. Chem. Lett.* **12**, 3733 (2021).
- [29] R. Dong *et al.*, A coronene-based semiconducting two-dimensional metal-organic framework with ferromagnetic behavior, *Nat. Commun.* **9**, 2637 (2018).
- [30] J.-H. Dou, L. Sun, Y. Ge, W. Li, C. H. Hendon, J. Li, S. Gul, J. Yano, E. A. Stach, and M. Dincă, Signature of metallic behavior in the metal-organic frameworks $M_3(\text{hexaiminobenzene})_2$ ($M = \text{Ni}, \text{Cu}$), *J. Am. Chem. Soc.* **139**, 13608 (2017).
- [31] D. L. Bergman, C. Wu, and L. Balents, Band touching from real-space topology in frustrated hopping models, *Phys. Rev. B Condens. Matter Mater. Phys.* **78** (2008).
- [32] Y. Hwang, J.-W. Rhim, and B.-J. Yang, General construction of flat bands with and without band crossings based on wave function singularity, *Phys. Rev. B* **104**, 085144 (2021).
- [33] A. C. Jacko, C. Janani, K. Koepernik, and B. J. Powell, Emergence of quasi-one-dimensional physics in a nearly-isotropic three-dimensional molecular crystal: Ab initio modeling of $\text{Mo}_3\text{S}_7(\text{dmit})_3$, *Phys. Rev. B* **91**, 125140 (2015).
- [34] C. Barreateau, F. Ducastelle, and T. Mallah, A bird's eye view on the flat and conic band world of the honeycomb and kagome lattices: towards an understanding of 2D metal-organic frameworks electronic structure, *J. Phys.: Condens. Matter* **29**, 465302 (2017).
- [35] E. P. Kenny, A. C. Jacko, and B. J. Powell, Tight-binding approach to pyrazine-mediated superexchange in copper-pyrazine antiferromagnets, *Inorg. Chem.* **60**, 11907 (2021).
- [36] M. Fuchs, P. Liu, T. Schwemmer, G. Sangiovanni, R. Thomale, C. Franchini, and D. D. Sante, Kagome metal-organic frameworks as a platform for strongly correlated electrons, *J. Phys.: Mater.* **3**, 025001 (2020).
- [37] See Supplemental Material at [URL_will_be_inserted_by_publisher](#) for details of the compact localized states when ligand-ligand hopping is included, additional details of the slave boson theory of superconductivity, and classification of the superconducting and nematic symmetries of the kagome-Lieb lattice.
- [38] J. C. Slater and G. F. Koster, Simplified LCAO method for the periodic potential problem, *Phys. Rev.* **94**, 1498 (1954).
- [39] P. Koskinen and V. Mäkinen, Density-functional tight-binding for beginners, *Comput. Mater. Sci.* **47**, 237 (2009).
- [40] G. Kotliar and A. E. Ruckenstein, New functional integral approach to strongly correlated fermi systems: The gutzwiller approximation as a saddle point, *Phys. Rev. Lett.* **57**, 1362 (1986).
- [41] G. Kotliar and J. Liu, Superexchange mechanism and d-wave superconductivity, *Phys. Rev. B* **38**, 5142 (1988).
- [42] S. Peotta and P. Törmä, Superfluidity in topologically nontrivial flat bands, *Nat. Commun.* **6**, 8944 (2015).
- [43] A. Julku, S. Peotta, T. I. Vanhala, D.-H. Kim, and P. Törmä, Geometric Origin of Superfluidity in the Lieb-Lattice Flat Band, *Phys. Rev. Lett.* **117**, 045303 (2016).
- [44] L. Liang, T. I. Vanhala, S. Peotta, T. Siro, A. Harju, and P. Törmä, Band geometry, Berry curvature, and superfluid weight, *Phys. Rev. B* **95**, 024515 (2017).
- [45] P. Törmä, L. Liang, and S. Peotta, Quantum metric and effective mass of a two-body bound state in a flat band, *Phys. Rev. B* **98**, 220511(R) (2018).
- [46] K.-E. Huhtinen, J. Herzog-Arbeitman, A. Chew, B. A. Bernevig, and P. Törmä, Revisiting flat band superconductivity: Dependence on minimal quantum metric and band touchings, *Phys. Rev. B* **106**, 014518 (2022).
- [47] J. Merino, B. J. Powell, and R. H. McKenzie, Ferromagnetism, paramagnetism, and a Curie-Weiss metal in an electron-doped Hubbard model on a triangular lattice, *Phys. Rev. B* **73**, 235107 (2006).
- [48] J. Lowe, *Quantum Chemistry* (Elsevier, London, 2012).

Supplementary Information: Flat bands and unconventional superconductivity in a simple model of metal-organic frameworks

I. COMPACT LOCALIZED STATES WITH LIGAND-LIGAND HOPPING

For $t_{LT} \neq 0$, $t_{LH} = 0$, two of the non-bonding bands develop a weak dispersion, (Fig. 3d), and the energy of the remaining exactly flat non-bonding band shifts to $E_{n_1} = t_{LT}$. The two kagome-like IFBs also remain flat. We can understand why these bands remain flat by examining their localized wavefunctions, Fig. 2a-c. First consider the model with $t_{LT} \neq 0$ and all other parameters set to zero. The model now consists of disconnected triangles of ligand sites. A single triangle has a bonding orbital with energy $-2t_{LT}$, and two antibonding orbitals of energy t_{LT} [1]. $|n_1\rangle_h$ is a linear superposition of these triangular antibonding orbitals on six triangles, therefore it is an eigenstate with energy t_{LT} . We have seen above that $|n_1\rangle_h$ is a zero energy eigenstate of the terms proportional to t , δ , and t_m . Therefore, $|n_1\rangle_h$ is an eigenstate of the full model with $t_{LH} = 0$ with energy t_{LT} . A similar argument explains why $|+\rangle_h$ and $|-\rangle_h$, which can be viewed as superpositions of the triangular antibonding states and atomic metal states, are eigenstates. $|n_2\rangle_h$ and $|n_3\rangle_h$ are no longer eigenstates, as ligand-ligand hopping across a triangle results in a non-zero amplitude on sites where the wavefunctions previously vanished, Fig. 2d,e.

For $t_{LT} = 0$, $t_{LH} \neq 0$, only one of the non-bonding bands remains exactly flat, with an energy of $E_{n_3} = 2t_{LH}$, Fig. 3e. This can be readily understood, as the model with $t_{LH} \neq 0$ and all other parameters set to zero consists of disconnected hexagons connecting ligand sites; and $|n_3\rangle_h$ is highest energy antibonding state of the tight-binding model on a single hexagon, Fig. 2e [2]. The other four localized states are not eigenstates for $t_{LH} \neq 0$, Fig. 2a-d.

II. SLAVE BOSON THEORY OF SUPERCONDUCTIVITY

The slave boson theory follows the procedure outlined in Refs. [3, 4] for the t - J model, Eq. (2), with isotropic nearest-neighbor hopping and an s -orbital per site. Ref. [4] applies the slave boson method to an s -orbital per unit cell, but inequivalent sites within the unit cell are treated as orbitals so a multiorbital extension is necessary for the kagome-Lieb lattice. The details of that extension are presented here.

A spinless auxiliary boson, \hat{b}_i , and fermion of spin σ , $\hat{f}_{i\sigma}$, are introduced for each site i . A faithful representation of the electronic operators is $\hat{c}_{i\sigma} = \hat{b}_i^\dagger \hat{f}_{i\sigma}$. With the interpretation that the bosons occupy only sites empty of electrons, the Gutzwiller projector is represented as a

set of constraints,

$$\sum_{\sigma} \hat{f}_{i\sigma}^\dagger \hat{f}_{i\sigma} + \hat{b}_i^\dagger \hat{b}_i = 1, \quad (\text{S1})$$

which are enforced by Lagrange multipliers, λ_i , on each lattice site. As in Ref. [4] a single Lagrange multiplier λ is used to make the problem tractable, which is equivalent to enforcing the constraint only on average. In order to reproduce the correct solution at half filling we renormalize $J \rightarrow \frac{3}{2}J$ [4].

A Hartree-Fock-Gorkov mean-field factorisation is performed, introducing the electronic superconducting, $\tilde{\Delta}_{ij} = (3J/8)\langle \hat{b}_i^\dagger \hat{b}_j^\dagger \rangle \langle \hat{f}_{i\uparrow} \hat{f}_{j\downarrow} - \hat{f}_{i\downarrow} \hat{f}_{j\uparrow} \rangle \equiv (3J/8)\langle \hat{b}_i^\dagger \hat{b}_j^\dagger \rangle \Delta_{ij}$, and quasiparticle nematic, $\chi_{ij} = (3J/8)\sum_{\sigma} \langle \hat{f}_{i\sigma}^\dagger \hat{f}_{j\sigma} \rangle$, order parameters, which are calculated self-consistently. Furthermore, the bosons are assumed to condense so that the boson operators are replaced with their expectation values. In Ref. [4], quadratic boson terms are simply the hole doping level, $\hat{b}_i^\dagger \hat{b}_j = 1 - n$. This is not directly applicable to our model as it contains two distinct types of site (metals and ligands). Instead, we assume that the phase of the bosons on each site is equal, giving $\hat{b}_i^\dagger \hat{b}_j = \sqrt{(1 - n_i)(1 - n_j)}$. Finally, at the mean-field level, the on-site energy of the metals in Eq. (1) can be written in terms of the doping levels as $\delta \sum_{i \in M, \sigma} \langle \hat{c}_{i\sigma}^\dagger \hat{c}_{i\sigma} \rangle = \delta \sum_{i \in M} n_i$.

The resulting mean-field Hamiltonian is quadratic and can always be diagonalized to find the energy. Doing so analytically on the kagome-Lieb lattice is impractical due to the dimension of the Hamiltonian, so the Hamiltonian is instead diagonalized numerically. Quantities such as the energy can then be calculated by integrating over the Brillouin zone allowing the ground state to be identified at zero temperature. Expectation values of the auxiliary fermion operators, such as those that appear in the order parameters, are calculated from the elements of the unitary matrix that diagonalizes the Hamiltonian. This allows for a simple self-consistent procedure following from an initial guess of Δ_{ij} and χ_{ij} where the total hole doping is fixed and the doping on each inequivalent site is calculated from the auxiliary fermion expectation values.

A. Symmetry of order parameters on the kagome-Lieb lattice

Because the unit cell of the kagome-Lieb lattice contains many sites, it is useful to enforce symmetries of the order parameters to reduce the number of self-consistent parameters. This is represented mathematically as $\Delta_{ij} = \eta_{ij}^\Delta \Delta$ and $\chi_{ij} = \eta_{ij}^\chi \chi$, where the η are the elements of the

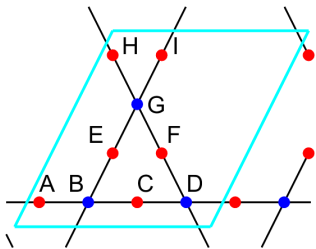


FIG. S1. Site labels of the kagome-Lieb lattice used to define the basis symmetry vectors (cf. Table S1).

normalized ‘symmetry vector’, which are fixed to constrain the symmetry of the order parameter. We assume all unit cells are equivalent and label the sites within each cell as shown in Fig. S1. A basis for the symmetry vectors is derived from the irreducible representations of the point group C_{6v} , which encompasses the symmetries of the kagome-Lieb lattice. By convention, these basis symmetries are labelled in analogy to the spherical harmonics (s, p, d, \dots) and are shown in Table S1. The primed symmetries are a second orthogonal set of basis symmetry vectors corresponding to the same irreducible representation.

Linear combinations of these basis vectors can also be taken. In the case where there are two symmetry vectors representing the same symmetry, such as p_x and p'_x , the two are allowed to mix. This introduces an extra self-consistent parameter but the problem remains tractable. This procedure was also used to test the symmetries $p_x + ip_y$ and $d_{xy} + id_{x^2-y^2}$, for example by mixing the two symmetry vectors $p_x + ip_y$ and $p'_x + ip'_y$.

While we allow for nematic order in our calculations we always find that the ground states are isotropic (s representation) where $\eta_{ij}^x = 1 \forall i, j$. Hence, in the main text, we only report the superconducting order parameters in the phase diagram.

III. MULTI-ORBITAL MODEL

We use the Slater-Koster method [5] to calculate hopping amplitudes between pseudo-atomic orbitals to parameterize the tight-binding Hamiltonian given by Eq. (1). We consider π -orbitals on the ligands (L) and d -orbitals on the metals (M), with possible nearest-neighbor hopping between pairs of M-L, M-M, and L-L. The functions determining the relevant hoppings can be obtained from Table I of Ref. [5] or Table 4 of Ref. [6], where we treat the π -orbitals of the ligands as p -orbitals.

For brevity, we illustrate below how one of the hopping amplitudes is obtained, with the hopping amplitude between other orbitals acquired in a similar manner. The hopping amplitude between a π_x orbital and a d_{xy} orbital

is given by

$$t_{x,xy} = \sqrt{3}l^2 m V_{pd\sigma} + m(1 - 2l^2)V_{pd\pi}, \quad (\text{S2})$$

which depends only on the unit displacement vector between the orbitals, $\hat{d} = (l, m, n)$, where l, m, n are the x, y and z components determined from the center of the metals and ligands on the kagome-Lieb lattice; and constants, $V_{\eta\zeta\beta}$, which depend on the type of orbitals the electron is hopping between ($\eta, \zeta = s, p, d$) and the bonding character between those orbitals ($\beta = \sigma, \pi, \delta$). The constants $V_{\eta\zeta\beta}$ are treated as free parameters that depends on the characteristics of the material of interest, and we include an on-orbital energy level, δ_μ , on the d -orbitals.

The parameters that produce Fig. 4 are given in Table S2. These were chosen by visual inspection to qualitatively match the band structure of Cu-BHT [7]. To limit the search in such a large parameter space we constrained δ_μ and $V_{\eta\zeta\beta}$ based on some physical considerations. The choice of the set $\{\delta_\mu\}$ is constrained as we require it to reproduce the expected orbital energies of the approximately square planar inner coordination sphere of the kagome-Lieb lattice. $V_{\eta\zeta\beta}$ is often a decaying function of distance, such that next-nearest-neighbor hopping can be an order of magnitude smaller than nearest-neighbor hopping. However, in many MOFs M-M hopping can be comparable in strength to M-L hopping [8]. Hence, in our parameter search we chose hopping strengths $M-L \geq M-M \gg L-L$.

In Fig. 4 we show the evolution of the band structure from the simplest multiorbital model with nearest neighbor hopping only to a model that closely resembles Cu-BHT. Note that the 6 nearly flat bands remain throughout. This shows that the flat bands in our model of Cu-BHT arise from Sutherland’s theorem.

	p_x	p_y	p'_y	p'_x	d_{xy}	$d_{x^2-y^2}$	$d'_{x^2-y^2}$	d'_{xy}	s	i	$f_{x(x^2-3y^2)}$	$f_{y(3x^2-y^2)}$
η_{AB}	-1	1	-1	1	-1	1	-1	-1	1	1	1	1
η_{BC}	1	-1	1	-1	-1	1	-1	-1	1	1	-1	-1
η_{CD}	-1	-1	1	1	1	1	-1	1	1	-1	1	-1
η_{DA}	1	1	-1	-1	1	1	-1	1	1	-1	-1	1
η_{BE}	2	0	-2	0	-2	0	2	0	1	-1	1	-1
η_{EG}	1	1	1	1	-1	-1	-1	1	1	1	-1	-1
η_{GI}	-1	-1	-1	-1	-1	-1	-1	1	1	1	1	1
η_{IB}	-2	0	2	0	-2	0	2	0	1	-1	-1	1
η_{DF}	-2	0	-2	0	2	0	2	0	1	1	-1	-1
η_{FG}	-1	1	1	-1	1	-1	-1	-1	1	-1	1	-1
η_{GH}	1	-1	-1	1	1	-1	-1	-1	1	-1	-1	1
η_{HD}	2	0	2	0	2	0	2	0	1	1	1	1

TABLE S1. Unnormalised basis symmetry vectors of the kagome-Lieb lattice belonging to two-dimensional representations of the point group C_{6v} . Site labels within a unit cell are shown in Fig. S1.

	$V_{pd\sigma}$	$V_{pd\pi}$	$V_{dd\sigma}$	$V_{dd\pi}$	$V_{dd\delta}$	$V_{pp\sigma}$	$V_{pp\pi}$
Even	1	1	0.5	0.3	0.2	0.05	0.05
Odd	0	1	0	-1	0.3	0.05	0

TABLE S2. Slater-Koster energy integrals, $V_{\eta\xi\beta}$, used in Fig. 4. The set of even (odd) orbitals is $\pi_x, \pi_y, d_{xy}, d_{x^2-y^2}$ (π_z, d_{xz}, d_{yz}). The on-orbital energies of the d -orbitals are $\delta_{xz} = \delta_{yz} = 0.5$, $\delta_{xy} = 1.5$ and $\delta_{x^2-y^2} = 4.5$, and we set the nearest-neighbor ligand-ligand hopping within hexagons and triangles equal (parameterized by $V_{pp\sigma}$ and $V_{pp\pi}$).

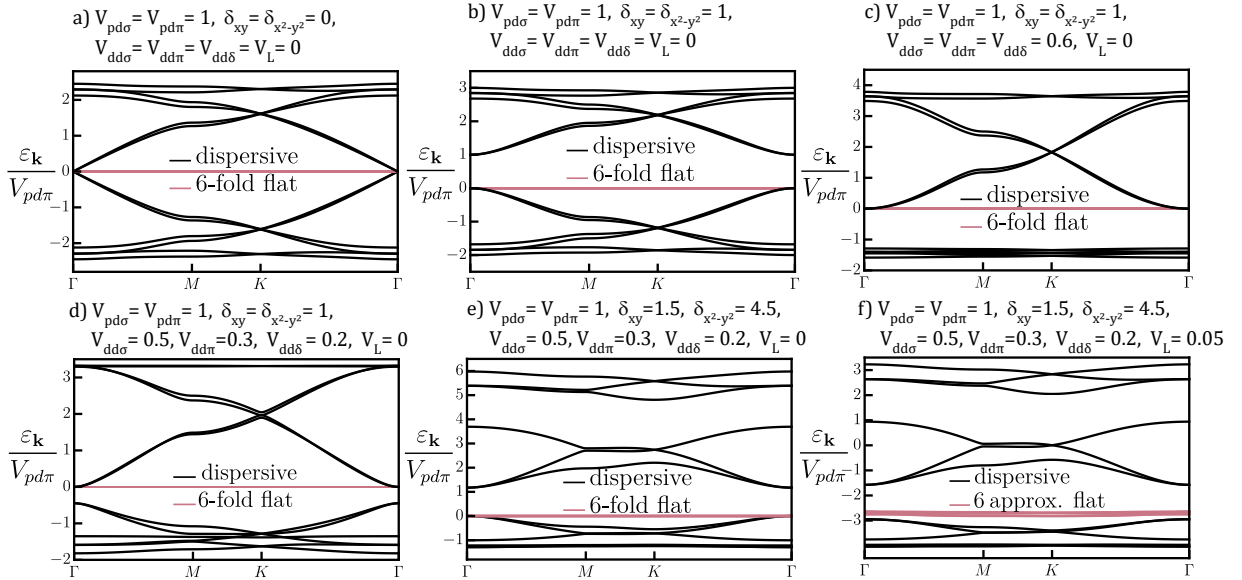


FIG. S2. Evolution of the bands arising from the even orbitals as Slater-Koster parameterized M-L, M-M, and L-L hopping are varied. In (a) there is only M-L hopping, (b) includes an on-orbital energy on the d -orbitals, (c) introduces M-M hopping that is equal for all d orbitals, (d) has unequal M-M hopping, (e) splits the on-orbital energy of the d -orbitals, and (f) introduces L-L hopping. (f) reproduces the even set of bands in Fig. 4, and we have shifted the energies to match the chemical potential in the band structure of Cu-BHT [7].

-
- [1] J. Merino, B. J. Powell, and R. H. McKenzie, Ferromagnetism, paramagnetism, and a Curie-Weiss metal in an electron-doped Hubbard model on a triangular lattice, *Phys. Rev. B* **73**, 235107 (2006).
 - [2] J. Lowe, *Quantum Chemistry* (Elsevier, London, 2012).
 - [3] G. Kotliar and A. E. Ruckenstein, New functional integral approach to strongly correlated fermi systems: The gutzwiller approximation as a saddle point, *Phys. Rev. Lett.* **57**, 1362 (1986).
 - [4] G. Kotliar and J. Liu, Superexchange mechanism and d-wave superconductivity, *Phys. Rev. B* **38**, 5142 (1988).
 - [5] J. C. Slater and G. F. Koster, Simplified LCAO method for the periodic potential problem, *Phys. Rev.* **94**, 1498 (1954).
 - [6] P. Koskinen and V. Mäkinen, Density-functional tight-binding for beginners, *Comput. Mater. Sci.* **47**, 237 (2009).
 - [7] X. Zhang, Y. Zhou, B. Cui, M. Zhao, and F. Liu, Theoretical discovery of a superconducting two-dimensional metal-organic framework, *Nano Lett.* **17**, 6166 (2017).
 - [8] E. P. Kenny, A. C. Jacko, and B. J. Powell, Tight-binding approach to pyrazine-mediated superexchange in copper-pyrazine antiferromagnets, *Inorg. Chem.* **60**, 11907 (2021).